

A Keck/HIRES¹ Study of Kinematics of the Cold Interstellar Medium in Dwarf Starburst Galaxies.

Colleen M. Schwartz² and Crystal L. Martin^{3,4,5}

Department of Physics, University of California, Santa Barbara, CA 93106

ABSTRACT

We have obtained high resolution Echelle spectra ($R = 30,000 - 50,000$) of the Na D absorption doublet ($\lambda\lambda 5890, 5896$) for six dwarf starburst galaxies and two more luminous starbursts: M82 and NGC 1614. The absorption features were separated into multiple components and separated into stellar and interstellar parts based on kinematics. We find that three of the dwarfs show outflows, with an average blueshift of 27 km s^{-1} . This is small compared to the highest velocity components in NGC 1614 and M82 (blueshifted by 150 km s^{-1} and 91 km s^{-1} , respectively); these two brighter galaxies also show more complex absorption profiles than the dwarfs. None of the outflow speeds clearly exceed the escape velocity of the host galaxy. Sightlines in NGC 2363 and NGC 4214 apparently intersect expanding shells. We compare the shocked gas velocity (v_{NaD}) to the ionized gas velocity ($v_{H\alpha}$) and interpret the velocity difference as either a trapped ionization front (NGC 4214) or a leaky H II region (NGC 2363). The dwarfs show $N_{NaD} = 10^{11.8-13.7} \text{ cm}^{-2}$, while the Na D columns in M82 and NGC 1614 are $10^{13.7} \text{ cm}^{-2}$ and $10^{14.0} \text{ cm}^{-2}$, respectively. The mass of expelled gas is highly sensitive to outflow geometry, dust depletion, and ionization fraction, but with a simple shell model we estimate neutral outflow gas masses from $\sim 10^6 M_{\odot}$ to $\sim 10^{10} M_{\odot}$.

Subject headings: galaxies: dwarf – galaxies: ISM – galaxies: kinematics and dynamics – galaxies: starburst – stars: formation

¹Data presented herein were obtained at the W.M. Keck Observatory, which is operated as a scientific partnership among the California Institute of Technology, the University of California and the National Aeronautics and Space Administration. The Observatory was made possible by the generous financial support of the W.M. Keck Foundation.

²colleen@physics.ucsb.edu

³cmartin@physics.ucsb.edu

⁴Packard Fellow

⁵Alfred P. Sloan Foundation Fellow

1. Introduction

Galactic winds are driven by supernovae and stellar winds in starburst galaxies. They drive outflows of metals and dust from the interstellar medium (ISM) into the galactic halo and even into the intergalactic medium (IGM). These outflows may also heat the intracluster medium and enrich it with metals, although the amount of matter permanently escaping the galaxy is still debated. The amount of interstellar gas expelled into the IGM by a starburst in a “blowout” is thought to depend on the star formation rate within the galaxy, the escape velocity of the galaxy, and the presence of an extended, low-density gaseous halo (Silich & Tenorio-Tagle 1998; Legrand et al. 2001). In dwarf starbursts, the mass-loss measurements have focused on the ionized components of this multi-phase flow. In this paper, we explore the kinematics of the cold, neutral clouds in dwarf starburst outflows.

Due to their low gravitational potential, dwarf starburst galaxies have small binding energies and may be particularly vulnerable to large mass loss via superwinds. Previous works have studied X-ray emission from hot gas within the starbursts (Dahlem, Weaver, & Heckman 1998; Martin, Kobulnicky, & Heckman 2002), and optical line emission (e.g. Lehnert & Heckman 1996) and absorption (Martin & Armus 2004; Rupke, Vielleux, & Sanders 2002; Heckman et al. 2000 - hereafter HLSA) from larger, more luminous galaxies. Other studies have observed dwarf galaxies in emission (Marlowe et al. 1995; Martin 1999), but ours is among the first to study dwarf starbursts in neutral absorption lines at optical wavelengths. We present a small sample of dwarf starburst galaxies and attempt to quantify mass flux in the cold neutral medium (CNM).

The advantage of looking at absorption lines is that we can eliminate all ambiguity in the direction of the radial flow of gas. Using the starburst itself as a background continuum source, it is known absolutely whether the gas we see in absorption is falling in (redshifted) or expanding outward (blueshifted). Moreover, unlike emission lines, whose strength scales as density squared, the strength of spectral lines seen in absorption are directly proportional to the column density of the neutral gas along the line of sight. Several previous studies (Phillips 1993; Lequeux et al. 1995; Gonzalez-Delgado et al. 1998; HLSA; Martin & Armus 2004) have detected interstellar absorption lines in starburst galaxies of various sizes and morphologies, finding blueshifted neutral gas and related large-scale outflows of metals. HLSA find an average outflow speed of $\sim 100 \text{ km s}^{-1}$ for luminous infrared galaxies (LIRGs) and more recently, Martin & Armus (2004) and Rupke et al. (2002) find outflow speeds of up to 700 km s^{-1} for two samples of ultraluminous infrared galaxies (ULIRGs).

We focus our observations on the Na I absorption doublet (5889.95 \AA and 5895.92 \AA , also called the Na D doublet) because it is stronger than any other optical resonance line (e.g. K I, Ca II); most other cosmically abundant resonance lines are produced in the UV

and therefore cannot be observed in nearby galaxies with ground-based telescopes. Na D is a good tracer of cold neutral gas because its ionization potential (5.14 eV) is less than that of hydrogen, so we can be sure any Na I absorption is occurring in a cold region of the ISM. It is also important to note that sodium is not as strongly depleted in diffuse, low-velocity clouds as K I or Ca II (Spitzer 1968; Savage & Sembach 1996). By using high resolution spectroscopy we can resolve individual, kinematically distinct doublet components within the absorption profiles. At lower resolution, deconvolving the absorption components of disparate origins is a more difficult task (see, e.g., HLSA).

It is our goal to observationally determine the kinematics of the CNM in our sample of starburst galaxies. In the second section of this paper, we discuss the observations, data reduction, and basic data analysis. In §3 we detail our method of separating stellar and interstellar sodium, discuss the kinematics and widths of the absorption features, and then use the interstellar sodium to determine a column density. In §4 we present our interpretation of the data, including simple models for outflow scenarios in the individual galaxies. The final section summarizes our major results.

2. Observations & Data Reduction

We observed eight nearby galaxies using the Keck I High Resolution Echelle Spectrometer (HIRES; Vogt et al. 1994) on 3-5 February 2000. Table 1 lists relevant properties of the galaxies. Six of the eight galaxies in the sample are classified as dwarfs; we define dwarf galaxies to have $M_B \geq -18$ for our choice of $H_0 = 75 \text{ km s}^{-1} \text{ Mpc}^{-1}$. NGC 1614 is a LIRG (Alonso-Herrero et al. 2001). M82 is slightly brighter than a dwarf galaxy, but less luminous than a LIRG, making it a good object with which to study the transition between the dwarfs and the LIRGs (Sofue 1997). The dwarf galaxies were selected mainly for compatibility with Martin 1998, which provides reference $H\alpha$ ($\lambda 6563$) narrowband images as well as preselecting galaxies with intense star formation over the range $-13.5 < M_B < -18.5$. The sample of galaxies observed here are also seen in $H\alpha$ to contain expanding supershells of ionized gas. NGC 1614 was not observed in that study, but does have large-scale $H\alpha$ structure (Neff et al. 1990). The slit in Martin’s 1998 observations missed the bubble in NGC 5253; however, this galaxy was seen to contain an expanding shell in $H\alpha$ by Marlowe et al. (1995).

The galaxies were observed with HIRES using both the red and blue cross dispersers to obtain full coverage of the desired wavelength range (i.e. from Ca II to K I). The red cross disperser covered the spectral range $5400 \text{ \AA} - 7700 \text{ \AA}$; the blue cross-disperser produced spectra in the range $3700 \text{ \AA} - 5900 \text{ \AA}$, with Echelle orders overlapping in wavelength to give complete spectral coverage to $\sim 5000 \text{ \AA}$. One galaxy, NGC 4214, was observed at two

positions, hereafter called NGC 4214-1 and NGC 4214-2 (a bright star cluster at the galactic nucleus and a cluster of star-forming knots, respectively – see §4.2.4). NGC 4214-2 was not observed with the blue cross-disperser. In all galaxies, the slit covered the brightest optical cluster to give the strongest continuum source against which to measure the absorption. Decker A12 was used; the slit size was $10'' \times 0.73''$ for NGC 1614 and NGC 4449, and $10'' \times 1.24''$ for all other galaxies.

The spectra were processed with the ECHELLE package in IRAF¹ using standard techniques. The CCD chip overscan region was used to bias-subtract the images, and a quartz lamp was used to flat-field the images in CCDPROC. Cosmic rays were removed from the CCD images by averaging multiple images of the same galaxy taken in succession on the same night; if multiple frames were unavailable, the IRAF task COSMICRAY was used to remove singular, bright pixels from the image. We did not flux-calibrate the spectra, as we are concerned primarily with measuring the equivalent width of absorption lines, which are purely a function of the normalized continuum intensity (Spitzer 1978). A Thorium-Argon lamp was observed for spectral wavelength calibration, resulting in rms residuals in each echelle order of less than 0.5 km s^{-1} . The resolution of the spectrum is 11 km s^{-1} (6 km s^{-1}) for the $1.24''$ ($0.73''$) slit, as measured from night sky lines. After the orders were extracted and the sky background was subtracted using the task DOECSLIT, the spectrum for each order was divided by the continuum to provide a normalized spectrum. The absorption line profiles were fit with Gaussian components using the IRAF task SPECFIT (Kriss 1994). This allowed us to fit multiple pairs of sodium lines to each profile and accurately measure the equivalent width of the lines.

3. Results

The Na D doublet was detected in six of the eight galaxies: NGC 1569, NGC 1614, NGC 4214-1 and -2, NGC 4449, NGC 5253, and M82. No absorption was seen in NGC 2363 or I Zw 18. We believe the Na D in NGC 5253, NGC 4214-1, and specific components of NGC 1569 and NGC 4449 are likely stellar in nature, via arguments discussed in section 3.1. The spectra of the five galaxies in which interstellar sodium absorption was detected are shown in Figure 1; there are a total of ten interstellar Na D absorption components.

It is interesting to compare the absorption line kinematics to those of emission-line gas.

¹IRAF (Image Reduction and Analysis Facility) is distributed by the National Optical Astronomy Observatories, which are operated by AURA, Inc., under cooperative agreement with the National Science Foundation.

H α kinematics were previously measured across large regions in the dwarfs in this paper and M82 to map out superbubbles by Martin 1998. Our observations directly measured the H α also – albeit over a much smaller region. Nonetheless, we can use the H α along these particular sightlines to tie Na D kinematics into these larger structures. The detailed results of these spectra will be discussed individually in §4.2

3.1. Stellar and Interstellar Sodium

In order to make a statement about the properties of the interstellar sodium in these galaxies, we need to first determine that the sodium we see is actually interstellar. The Na D resonance doublet is prominent in the spectra of cooler stars. The spectrum of a dwarf will be dominated by K-type giants and supergiants if the starburst is older than ~ 10 Myr (Leitherer et al. 1999); these stars show strong photospheric sodium absorption. Therefore, we must find a way of deciphering the nature of the neutral sodium observed.

We have made use of the available stellar spectral lines in our data to help distinguish between stellar and interstellar sodium. In particular, the Mg b band triplet (5167.32 Å, 5172.68 Å, and 5183.60 Å) is a good indicator of the presence of certain stellar populations. The Mg b triplet is present in F through M stars, with maximum absorption in the range K0 to M3, and is not present in the CNM because it is a highly excited line. Therefore, we can be certain that any Mg b absorption we see is from a stellar atmosphere. The equivalent width of this absorption feature is also well correlated with that of the stellar Na D absorption; we can use the Mg b to disjoin the stellar and interstellar sodium by fitting the Na D absorption profiles with multiple components, one of which corresponds to a purely stellar feature.

Using the stellar atlas of Jacoby, Hunter, & Christian (1984), we have measured the equivalent widths of the Mg b and Na D absorption lines in a sample of stars and fit the data with a least-squares fit. We find

$$W(\text{NaD}) = (0.40 \pm 0.05) \times W(\text{Mgb}) + (0.65 \pm 0.28). \quad (1)$$

This is shown with the data from the stellar atlas in Figure 2. This is consistent with the calculations of Rupke et al. (2002) that $W(\text{NaD}) \sim 0.5W(\text{Mgb})$. We can use this relationship to predict the strength, width and velocity of the stellar component of the Na D absorption. There are two galaxies in our sample, NGC 1569 and NGC 4449, which have both a stellar and interstellar component. NGC 5253 has what appears to be a purely stellar component, and therefore is not included in the sample of galaxies showing interstellar neutral sodium absorption. The equivalent widths of the stellar and interstellar Na D and Mg b for these three galaxies are shown in Figure 3, and the Mg I spectra are presented in Figure 4. The

central component of the M82 absorption profile is near the systemic velocity (it is redshifted by only 4 km s^{-1}); however, no Mg b absorption is seen to a level of 0.24 \AA . Since the equivalent width of the Na D absorption in this central component is 1.44 \AA , we can safely say that there is no significant population of cool giants and supergiants contaminating the spectrum at this position, and we will assume this component is purely interstellar.

HLSA classify their “interstellar dominated” sample galaxies as having a larger line width than their “strong stellar contamination” galaxies. Since our spectra are well resolved and we are able to distinguish between stellar and interstellar lines, it is interesting to note that we can use this method, rather than the overall width of the absorption profile, to categorize the Na D. There are only two galaxies (NGC 1569 and NGC 4449) where we have both stellar and interstellar lines, and both of these absorption line systems have a larger interstellar width than stellar. Similarly, HLSA found that systems with larger widths are interstellar dominated.

3.2. Kinematics of the Interstellar Na I

To discuss the kinematics of the CNM, it is imperative to know the systemic velocity (v_{sys}) of the galaxy, i.e. the heliocentric velocity of the starburst. However, one may wish to compare data with previous observations in which the velocity of the galactic center of mass was used. Usually the center-of-mass velocity and the stellar velocity are similar, unless the galaxy is inclined and the starburst region is far from the axis of rotation; this could create a velocity offset between the starburst velocity and that of the galactic nucleus. In this case, it may be better to use the velocity of the stars themselves. We were able to get stellar velocities for three galaxies (NGC 1569, NGC 4449, and NGC 5253) by using stellar absorption lines (see §3.1). In the other five galaxies, we set the systemic velocity using (in order of preference) CO maps (NGC 1614, NGC 4214, and M82), optical lines (NGC 2363), and stellar velocities (I Zw 18). Table 1 gives the systemic velocities used in this analysis and their sources. A heliocentric velocity scale is used throughout the paper.

The HLSA sample of 32 LIRGs showed significant blueshifts in the Na D doublet for their “interstellar dominated” outflows, indicating nuclear outflows with typical velocities of $\sim 100 \text{ km s}^{-1}$. Our data for the dwarf galaxies also show the Na D absorption to be blueshifted, although with overall slower outflow speeds ($\sim 30 \text{ km s}^{-1}$). NGC 1614 and M82 show both redshifted and blueshifted components; these are further discussed in §4.2. The velocities for individual interstellar absorption components are given in Table 2.

The line width (FWHM) of the interstellar components for the dwarfs and M82 ranges

from ~ 30 to ~ 80 km s $^{-1}$, with an average of 43 km s $^{-1}$. The existence of such broad absorption lines in neutral sodium leads us to conclude that there are multiple clouds of cold gas producing each component of the absorption; the thermal width of a cloud of cold gas at ~ 100 K would be only ~ 0.20 km s $^{-1}$. Moreover, the line widths of cold clouds in the Galactic halo are found to be just a few km s $^{-1}$ (Spitzer & Fitzpatrick 1995). The individual line widths in NGC 1614 are significantly larger (~ 100 km s $^{-1}$ or more) than those in the dwarfs or M82 (~ 45 km s $^{-1}$). The total width of all components in M82 is relatively large (236 km s $^{-1}$).

Among the dwarfs in the sample, we do not see a correlation between the FWHM of the lines and the rest-frame equivalent width. However, when the data for M82 and NGC 1614 are added, there is a trend wherein equivalent width increases in proportion to FWHM, for these N points. Given the lack of correlation seen by HLSA using a much larger data set, we conclude only that the largest values of FWHM (and similarly the largest equivalent widths) are much smaller in dwarfs than in brighter galaxies.

3.3. Column Densities

The doublet lines are fit with Gaussian profiles in pairs with SPECFIT to measure the velocity, FWHM, and equivalent width W of each line (see Table 2). If the absorbing gas is optically thin, then the blue ($\lambda 5890$) line will be twice as strong as the red ($\lambda 5896$) line, and the “doublet ratio,” $W_{blue}/W_{red} = 2$. If the gas is optically thick, W_{blue}/W_{red} approaches unity as the optical depth τ approaches infinity. In our data, just one component is optically thin, the rest are optically thick.

We can easily measure how much of the continuum source is being obscured by absorbing gas clouds by studying the residual normalized intensity I_λ of a line at wavelength λ . If $I_\lambda = 0$ for the blue line of a doublet (i.e. the stronger line), then no continuum radiation is “leaking” into the absorption line. In other words, the absorbing cloud completely covers the continuum source and the covering factor $C_f = 1$. If a cloud does not cover the whole source, the continuum radiation will “leak” into the absorption profile and increase the minimum flux, I_λ , and $C_f < 1$. Specifically, following the derivation of Barlow & Sargent (1997), we can find the covering factor:

$$C_f = \frac{I_{5896}^2 - 2I_{5896} + 1}{I_{5890} - 2I_{5896} + 1}. \quad (2)$$

In our data, the covering factor ranges from 0.23 to 1.0 (see Table 2).

Now that we know the covering factor of the absorbing gas, we can determine the Na D column density. The curve of growth relates the optical depth at line center, τ_0 , to the

doublet ratio via a function $F(\tau_0)$, determined numerically (Spitzer 1978). The column density is then

$$N = \left\{ \frac{\pi^{1/2} \tau_0}{2F(\tau_0)} \right\} 1.13 \times 10^{20} \frac{W_\lambda}{\lambda^2 f} \text{ cm}^{-2} \quad (3)$$

(Spitzer 1968), where f is the oscillator strength (Morton 1991), and W_λ and λ are given in Angstroms.

Using this method, we find that $N(\text{NaD})$ in the dwarfs ranges from $6.2 \times 10^{11} \text{ cm}^{-2}$ in NGC 1569 to $5.1 \times 10^{13} \text{ cm}^{-2}$ in NGC 4449. We find the total neutral sodium column densities in NGC 1614 and M82 to be $1.0 \times 10^{14} \text{ cm}^{-2}$ and $2.4 \times 10^{13} \text{ cm}^{-2}$, respectively. The measured equivalent widths, and the calculated covering factors and Na D column densities, are presented in Table 2. From the column density of sodium, we can then use the metallicity of the galaxy (given in Table 2; $(\text{Na}/\text{H})_\odot = 2.04 \times 10^{-6}$ – Martin & Zalubas 1981) to find the total H I column probed. A source of systematic uncertainty is the contingency of neutral sodium column density on the ionization parameter, f_{ion} , as well as the fractional depletion of sodium onto grains, f_D . Since dwarfs typically have a low metallicity, we expect lower dust content and depletion level than in larger galaxies. It is the product of these, $f_D f_{ion}$, which is the important factor in our calculations, as is seen in Wakker & Mathis (2000). They measure the abundance of neutral sodium in Galactic high- and intermediate-velocity clouds. Using their results and a typical H I column of 10^{20} cm^{-2} , we calculate $f_D f_{ion} = \sim 300$. We therefore parameterize the column densities by a simple factor of $(f_D f_{ion}/100)$ to reflect the typical correction, and calculate the total H I column using the equation

$$\frac{N(\text{Na I})}{N(\text{H I})} = \left(\frac{Na}{H} \right)_\odot \left(\frac{Z}{Z_\odot} \right) \frac{1}{f_D f_{ion}}. \quad (4)$$

We find that the corresponding $N(\text{H I})$ in the dwarfs could be as large as $10^{20}(f_D f_{ion}/100) \text{ cm}^{-2}$ (NGC 1569) to $10^{22}(f_D f_{ion}/100) \text{ cm}^{-2}$ (NGC 4449). In M82 and NGC 1614, this conversion gives a total H I column of $10^{21}(f_D f_{ion}/100) \text{ cm}^{-2}$ and $10^{22}(f_D f_{ion}/100) \text{ cm}^{-2}$, respectively.

3.4. Comparison to K I Absorption Spectra

In addition to Na D, the K I resonance absorption line ($\lambda\lambda 7664.91, 7698.97$) is also present in two of our spectra. K I and Na I have similar ionization potentials (4.34 eV and 5.14 eV, respectively) and similar depletion levels (Savage & Sembach 1991, Wakker & Mathis 2000), so it is expected that the species will be spatially coincident in the CNM. It is unfortunate that in nearby galaxies, K I is found in spectral regions that are strongly contaminated by the Fraunhofer A-band absorption from atmospheric O_2 (near 7600 Å). In

only two galaxies were we able to discern the K I absorption: NGC 1569 and NGC 1614. NGC 1569 is luckily blueshifted slightly away from the sky absorption, while NGC 1614 is redshifted out of the contaminated region entirely. Other galaxies are either completely contaminated by the Fraunhofer absorption, the K I doublet is too weak to measure, or the lines lie between Echelle orders.

The K I profile is arguably a better constraint on the cold gas kinematics than the Na D profile because the doublet spacing is wider, and the K I oscillator strength is lower so the lines are less saturated. We fit the K I profile in NGC 1614 with SPECFIT and found components at -149 km s^{-1} and $+70 \text{ km s}^{-1}$. This result helped us pin down the best component velocities for the Na D fits, which were previously poorly constrained. Due to the low signal-to-noise of the continuum, the doublet ratio and covering factor are uncertain. The results of the fitting are presented in Table 3.

Without the addition of K I, the Na D profile for NGC 1569 is blended with Galactic absorption and atmospheric emission. The stellar profile from the starburst is constrained by Mg I absorption, leaving a range of possibilities for the central velocity of the interstellar Na D. We find K I absorption at -24 km s^{-1} , thereby defining the velocity at which the interstellar Na D lies. Due to the Fraunhofer absorption, the normalization of the continuum in the NGC 1569 spectrum is likely imperfect and the column densities in Table 3 are highly uncertain. The K I spectra do not provide a useful column density constraint.

4. Dynamics of the Cold Neutral Gas

Although we sample just one sightline, we can estimate how much of the CNM is brought out into the outflow, if any. Only five of the sample galaxies show interstellar sodium absorption, just three of which are dwarfs. Due to the intricacies in geometry and modeling of the individual galaxies, as well as the small number of sample galaxies, it is preferable to look at each galaxy individually. Below we discuss the galaxies independently, detailing the information gleaned from their spectra, and presenting a model of the starburst kinematics and any outflow/infall structure. Ideally, we would like to be able to calculate the amount of cold, neutral gas flowing into the IGM, when possible. This requires knowledge not only of the kinematics and column densities, but also the geometry of the starbursting region itself.

4.1. Calculation of Superbubble Masses

One important application of measuring the column density of a superbubble or shell region around a starburst is to measure the mass of gas being expelled from the starburst. We can do this, so long as we make a few assumptions. We use the wind/bubble model introduced by Weaver et al. (1977), wherein a starburst is surrounded by concentric shells of (in order of increasing radius) a free-flowing wind, a shocked wind, and a shocked shell of neutral ISM. The Strömgren sphere of the stars may be trapped in the shell, or may completely photoionize the region. We postulate that the H α emission is found in the warm, dense ionized gas region, while the Na D absorption is found in the colder, shocked neutral gas region. This model is applicable in light of the expanding shells of warm gas seen in H α images by Martin 1998. We assume the shells are perfectly spherical, making the mass a function of the column density within the shell and the area of the shell. Given a shell of radius R , the mass of the shell in neutral hydrogen is

$$M(\text{H I}) = 4\pi R^2 N(\text{H I}) \mu m_H C_f^{-1}. \quad (5)$$

All of the following models use parameters (R , Z/Z_\odot) as are detailed in Table 4 and Na I column densities as given in Table 3 and transformed into $N(\text{H I})$ using Equation 4. The column densities assume ionization fractions and depletion parameters as discussed in §3.3, namely that $f_D f_{ion} = 100$.

4.2. Individual Galaxies

4.2.1. NGC 1569

The sightline to NGC1569 intersects the midplane of the disk. We observe the shell 1569-C in H α at a radius of $\sim 3''$ (32 pc) from the continuum source. This is most likely the same region in which Mühle et al. (2001) parameterized an H I “hole,” associated with the starburst, 1 kpc in diameter expanding at 7 km s $^{-1}$. The neutral gas outflow we observe in the nearby dwarf galaxy NGC 1569 is moving more slowly than the bipolar outflow seen in H α by Martin (1998). If we assume the neutral sodium is spatially coincident with the edge of this H I hole, i.e. the neutral sodium is swept up in a slowly expanding shell around the starbursting area, then we find the total mass of cold, neutral gas swept up to be $2.2 \times 10^7 M_\odot (R/100 \text{ pc})^2$. The H I mass of this galaxy is found from radio observations to be $8.4 \times 10^7 M_\odot$. Therefore, the neutral gas in the shell modeled is a small fraction ($\lesssim 10\%$) of the total neutral gas mass of the galaxy.

Martin et al. (2002) imaged NGC 1569 in X-rays with *Chandra* and argued that the

observed outflowing wind is strong enough to blow through the galactic halo. In fact, they found that nearly all of the metals ejected by the starburst are carried into the IGM by the galactic superwind, and are primarily from the stellar ejecta itself, not the entrained ISM. Therefore, it is not surprising that this galaxy shows the smallest amount of outflowing neutral gas of our entire sample. The outflowing mass is measured to be $1.4 \times 10^6 M_{\odot}$ in hot gas and $8.8 \times 10^6 M_{\odot}$ in warm gas (Martin 1998). In contrast, we find $2.2 \times 10^7 M_{\odot}$ in H I for a 500 pc (radius) shell.

From Mg b band absorption we know there must be a stellar component of the Na D profile at the systemic velocity. By fitting a corresponding stellar component to the Na D profile, and by fitting the atmospheric absorption and Galactic emission, we find there is one interstellar absorption component required for a good fit (see Figure 5). This gas, blueshifted 24 km s^{-1} from the systemic, corresponds to the K I absorption seen at the same velocity. We use a value of $v_{sys} = -40 \text{ km s}^{-1} \pm 0.6 \text{ km s}^{-1}$, obtained from the Mg b band absorption in the stellar atmospheres within the starburst. It is important to note that our value of the systemic velocity is somewhat lower than the typical values for this galaxy: Meier et al. (2001) used ^{12}CO to find a systemic velocity of -68 km s^{-1} , while Stil & Israel (2002) used the galaxy’s H I rotation curve to find a mean systemic velocity of -82 km s^{-1} . In fact, when comparing the heliocentric velocity of the Na D with the above values of the systemic velocity, it is possible that while the Na D is blueshifted in relation to the Mg I, it may be at the systemic velocity or even redshifted. Additional uncertainty in the analysis of the cold interstellar gas arises from possible absorption by neutral gas in intervening Galactic intermediate- or high-velocity clouds (Kuntz & Danly 1996). Moreover, H I in the Galactic thin disk is seen towards NGC 1569 (Hartmann & Burton 1997), and could overlap in velocity with the lines from NGC 1569.

4.2.2. NGC 1614

We observed NGC 1614 in order to extend our observations beyond the scale of dwarf galaxies and into a higher luminosity class. This relatively close LIRG ($D = 64 \text{ Mpc}$ for $H_0 = 75 \text{ km s}^{-1} \text{ Mpc}^{-1}$) has a violent starburst in the central region which is thought to have been triggered by interaction with another massive galaxy, as evidenced by outer structures including plumes, tails, and a possible secondary nucleus as seen by Alonso-Herrero et al. (2001). We observe the primary/nuclear starburst. The disk of this galaxy is inclined at $i = 51^\circ$ to the line of sight (Alonso-Herrero et al. 2001), so our sightline intersects the outflow.

Our observations of this galaxy successfully resolve the absorption profile into two sep-

arate components – a weaker outflowing component at -149 km s^{-1} , and a stronger infalling component at $+70 \text{ km s}^{-1}$. The spectra of Na I, K I $\lambda 7665$, and $\text{H}\alpha$ are shown, along with the individual components of Na I and K I, in Figure 6. Alonso-Herrero et al. (2001) use the integrated far-infrared luminosity of the galaxy to find a star formation rate of $52 \text{ M}_{\odot} \text{ yr}^{-1}$. Combined with their value of the total gas mass fueling the starburst ($3 \times 10^8 \text{ M}_{\odot}$), we find the starburst age to be 5.8 Myr. Using this age and the velocity of the outflowing neutral sodium absorption component, we can determine the radius of the shell assuming a constant velocity expansion. We find in this model that the outflowing component supports a shell 1 kpc in radius, with a total outflow mass of $2.1 \times 10^9 \text{ M}_{\odot} (R/1 \text{ kpc})^2$. Assuming the redshifted/infalling component is a spherical shell, we parameterize it in terms of a bubble with radius 1 kpc. This case gives a total infalling mass of $2.9 \times 10^9 \text{ M}_{\odot} (R/1 \text{ kpc})^2$. The total H I mass of this galaxy is given by Bushouse (1987) to be $1.7 \times 10^9 \text{ M}_{\odot}$, so the simple shell geometry cannot completely model the cold ISM of this galaxy.

This complex system is difficult to sort out. The completely uncoupled kinematics of the $\text{H}\alpha$ and Na D spectra suggests that the shock fronts and ionization fronts are moving independently. It is possible that we are seeing redshifted absorption due to neutral gas in one of the filaments of gas or spiral arms of the galaxy – the violent interaction of NGC 1614 colliding with another galaxy has created a complex system of filaments and hot spots which may cause the infall of cold, neutral gas. Alternatively, there may be separate continuum sources, one redshifted and one blueshifted, and at least one of which is offset from the galactic rotation axis.

4.2.3. NGC 2363

NGC 2363 is an extremely luminous giant H II region connected to NGC 2366. Our observations of the nuclear starburst show a very straightforward double-peaked emission line structure with components at an average velocity of 83 km s^{-1} and 107 km s^{-1} . This is in agreement with the models of Roy et al. (1991, and references therein), who observed this galaxy in [O III] ($\lambda 5007$) and also found very clear line splitting. We see no Na D absorption, and place an upper limit on the column density of $\text{N}(\text{Na I}) \leq 6 \times 10^{11} \text{ cm}^{-2}$.

With our emission line data – both spectra and echellegrams – we can support the claim of Roy et al. (1991) that there is a relatively simple system with one superbubble (presumably expanding) around this giant H II region. Our [O III] line splitting of 29.4 km s^{-1} (i.e. an expansion velocity of 14.7 km s^{-1}), compared with the data of Roy et al. (1991), leads us to believe that we are looking at a region about 7 arcsec – or a physical size of 122 pc at a given distance of 3.6 Mpc – from the center of the superbubble. From this distance

and the blending of the emission lines in our data, we can deduce that we are seeing the edge of the bubble. The difference in the size of the bubble given by our measurements and those of Roy et al. (1991) can be attributed to the difference in assumed distance to the galaxy. Our upper limit on the total mass of cold neutral gas is $1.2 \times 10^6 M_{\odot} (R/122 \text{ pc})^2$. The ionized mass of NGC 2363 was found by Luridiana, Peimbert, & Leitherer (1999) to be $3.4 \times 10^6 M_{\odot}$, which indicates that the outflowing cold gas is a small fraction of the galactic mass.

The absence of Na D absorption tells us that the ionization front created by the starburst may have “caught up” to the shock front, so that the ionization front is no longer trapped within the expanding shell. Hence, we find a lack of neutral gas, even though there is very obviously a shell present both in previous observations and in our H α observations. This results in a “leaky,” expanding H II region, with ionizing radiation escaping beyond the edge of the shell.

4.2.4. NGC 4214

This nearby dwarf galaxy went through a starburst phase which started roughly 10^7 years ago (Huchra et al. 1983). We observed two different positions in the galaxy, as discussed in §2. NGC 4214-1 (north-west complex, J2000 R.A.=12^h15^m39^s.48, Decl.=36°19′31″.00) corresponds to a bright super star cluster (SSC) and likely the galactic center, while NGC 4214-2 (south-east complex, R.A.=12^h15^m37^s.99, Decl.=36°19′44″.20) is made of several smaller star-forming knots. We will discuss these regions separately due to their disparate geometry and kinematics. Note that our positions NGC 4214-1 and -2 correspond to knots 1 and 2 of Sargent & Fillipenko (1991) and regions I and II in MacKenty et al. (2000).

NGC 4214-1

NGC 4214-1 is the brightest starburst knot in this galaxy. The central knot in this region is a massive SSC containing several hundred O stars (Leitherer et al. 1996; Sargent & Fillipenko 1991). Observations of ionized and neutral hydrogen around this massive star-forming site have found large cavities in the ISM, suggesting material was blown out of these areas by stellar winds and supernovae. The starburst can be characterized, using the stellar population, as an instantaneous starburst aged around 3.5 Myr (Cerviño & Mas-Hesse 1994).

No Mg I absorption is seen in this spectra as there is low signal-to-noise near the Mg b triplet. Additionally, the Na D absorption seen is at the local systemic velocity, so we cannot make a conclusive statement about the nature of the absorption. However, accounting for

the upper limit on both the equivalent width of Na D (0.04 Å) and Mg b (0.03 Å), we can say that upon comparison with equation (1) and Figure 3, it is highly likely that the Na D absorption seen is stellar. If this is not the case and the absorption is interstellar, then this may be an extension of the observations of Leitherer et al. (1996), who observe interstellar UV lines at the systemic velocity. Assuming the Na D absorption is completely interstellar (i.e. an upper limit), then the covering factor is 0.52 and the column density of Na I is $5.87 \times 10^{11} \text{ cm}^{-2}$. Assuming a bubble radius of 700 pc (an educated guess based on the H α morphology seen in Martin 1998), we find an upper limit on the mass of the stationary shell of $2.5 \times 10^7 M_{\odot} (R/700 \text{ pc})^2$.

NGC 4214-2

This region has a much different morphology than NGC 4214-1, with ionization by three small OB associations ($\sim 4,000$ roughly coeval OB stars observed as H α knots). Our H α profile is double-peaked, showing a bright emission line blueshifted from v_{sys} and a weaker redshifted component, suggesting an expanding shell in H α . Indeed, in looking at the H α echellegram, one can easily see the “hole” which indicates the center of the shell (see Figure 7). The Na D and H α spectra are plotted against velocity for NGC 4214-2 in Figure 8. Since we have no blue spectrum for this position, we cannot use Mg I to define the nature of the gas. However, the Na D profile is blueshifted from the local systemic velocity as given by CO (Becker et al. 1995); this leads us to believe the absorption is interstellar.

The neutral sodium is observed to be expanding at 23 km s^{-1} , with a width of 40 km s^{-1} . The H α and Na D profiles have the same Doppler width. The kinematics indicate that there is an expanding neutral shell and an ionized shell. The ionized shell is presumably interior to a concentric shell of neutral gas, and the H α shell seems to be expanding a few km s^{-1} faster than the Na D shell (i.e. is more blueshifted). Assuming a single, expanding shell, the total mass of neutral gas flowing out of NGC 4214-2 is $\sim 7.5 \times 10^7 M_{\odot} (R/500 \text{ pc})^2$.

NGC 4214 has a total H I mass of $1.9 \times 10^9 M_{\odot}$ (Kobulnicky & Skillman 1996; McIntyre 1998). The combined mass of the maximum possible outflow in NGC 4214-1 and the outflow in NGC 4214-2 is $\sim 10^8 M_{\odot}$. This indicates that while the outflow is significant, it is but a fraction of the total neutral ISM; its gas structure as a whole should be considerably affected by the starbursting region.

4.2.5. NGC 4449

This nearby galaxy has an unusually large B-band luminosity – brighter than any other dwarf in this sample (see Table 1). *Chandra* X-ray imaging shows an expanding superbubble within a cavity of $H\alpha$ emission in the region we observe (Summers et al. 2003), and H I observations show an unusually massive galactic halo (Bajaja, Huchtmeier, & Klein 1994). Imaging in $H\alpha$ (Martin 1998) shows a system of large shells breaking out along a nuclear bar structure, with smaller bubbles growing along the edge of the galactic disk. It is possible that these smaller bubbles merge into a larger bubble.

The HIRES spectra show that the cold, neutral gas in NGC 4449 is kinematically uncoupled from the warm, ionized gas as seen in $H\alpha$ (see Figure 9). The region we observe is the center of the $H\alpha$ emission (Hunter et al. 1998), and the neutral sodium we see expanding at 34 km s^{-1} is most likely a product of several superbubbles expanding out of the galactic plane along the line of sight. Indeed, the column density, $N_{NaD} = 5.1 \times 10^{13} (f_D f_{ion}/100) \text{ cm}^{-2}$, is larger than in any other dwarf. The unusually large sodium column may be due to additional neutral gas in the halo, explaining the existence of as much as 300 times more neutral matter in this galaxy as compared to NGC 1569 or NGC 4214 (Bajaja et al. 1994). If the CNM being expelled from the nuclear region is being pushed by the conglomerate effect of the $H\alpha$ bubbles, we can approximate the geometry of the neutral gas by a single bubble with a radius $\sim 1 \text{ kpc}$. This radius is on the order of the radius of the largest complex seen in $H\alpha$ imaging, which Martin (1998) calls NGC 4449-A (radius = 950 pc). Given the high column and radius, we find that this shell contains a total neutral gas mass of $7 \times 10^9 M_\odot (R/1 \text{ kpc})^2$. From radio observations, Bajaja et al. (1994) find a total galactic H I mass of $2.3 \times 10^9 M_\odot$, which suggests that we may be seeing the galaxy’s massive halo along our line of sight.

4.2.6. NGC 5253

We detect Na D absorption at a 3σ level in NGC 5253, but as discussed in §3.1, this absorption is believed to be stellar because it is at the same velocity as the Mg I absorption and it falls directly on the relation for stars (see Figure 3). Marlowe et al. (1995) observe two kpc-scale superbubbles in $H\alpha$ flanking the galactic center along its minor axis. We see these in emission only: a brighter line blueshifted by 39 km s^{-1} and a weaker line blueshifted by 73 km s^{-1} . Our sightline to the nuclear starburst (5253-1; Calzetti et al. 1997) could intersect either bubble, or both; the geometry is unclear. The upper limit on interstellar sodium absorption we detect is $N(NaD) = 2 \times 10^{11} \text{ cm}^{-2}$, which gives a mass of $\sim 10^7 M_\odot (R/870 \text{ pc})^2$ using the bubble radius seen in $H\alpha$ by Martin (1998). This is still a large amount

of mass, so this is by no means a definitive statement that there is no expanding shell; our sightline simply misses the shells as shown in Martin 1998 (Figure 2j in that paper). The H I mass of NGC 5253 is roughly $1.4 \times 10^8 M_\odot$ (Kobulnicky & Skillman 1995), indicating that the mass of cold outflowing gas detected is small compared to the total neutral gas mass of the galaxy.

4.2.7. M82

Our observations of Na D in M82 show an extremely complex absorption system, best fit with five separate absorption doublets. The two blueshifted components are the strongest; there is a single component within 4 km s^{-1} of the systemic velocity ($v_{sys} = 214 \text{ km s}^{-1}$ – see Table 1), and there are two fairly strong redshifted doublet lines. All of the components are highly saturated with the exception of the redmost component, which is optically thin (i.e. the doublet ratio = 2).

M82 is viewed edge-on, and our sightline intersects the nuclear region of the galactic disk. A bright, bipolar outflow is observed out to distances of $>11 \text{ kpc}$ along the minor axis of the galaxy (Lehnert, Heckman, & Weaver 1999). CO observations by Weiß et al. (1999), combined with the schematic diagram presented by Ohya et al. (2002, see their Figure 7), leads us to believe we are looking through several filaments separated by regions of warmer, nuclear emission. The CO images are centered on the most powerful supernova remnant in the galaxy, SNR 41.9+58, roughly $17''$ from our sightline (R.A.=09^h55^m53^s.1, Decl.=69°40′47″.2). Using our value of the systemic velocity (214 km s^{-1} , Lo et al. 1987), the most redshifted component in our Na D spectrum is at approximately the same velocity as the CO. This suggests that the redshifted atomic gas is absorption in the galactic disk close to the molecular gas, near the starburst.

H α images (Martin 1998) and H I images (Wills, Pedlar, & Muxlow 2002) show that a large, expanding superbubble is seen along the minor axis of the galaxy, and is likely made up of several smaller bubbles forming an outflow as they merge. We can make an educated guess on the distance from the continuum source to the Na I absorbing gas by using the ages derived from H α shell expansion in Martin (1998), and find the dynamical age of the shells to be $\sim 8 \text{ Myr}$. This gives shell sizes on the order of a few hundred pc. Assuming solar metallicity, we can find the mass expelled in the simple case of independently expanding spheres. The shells range in neutral gas mass from $\sim 5 \times 10^6 M_\odot (R/286 \text{ pc})^2$ to $8 \times 10^7 M_\odot (R/500 \text{ pc})^2$. These are relatively small compared to the other similarly luminous galaxies where Na I absorption is detected; it should be noted that the radii given, and therefore the masses, are a lower limit.

4.2.8. I Zw 18

I Zw 18 is important to study due to its extremely low metallicity - $O/H \approx 0.02(O/H)_\odot$ - and high H I column, making it a prime candidate for a young galaxy undergoing its first phase of star formation (Lequeux et al. 1979). Moreover, the galaxy has a relatively low escape velocity, and feedback from star formation could drastically affect the galaxy (Martin 1996). We observed I Zw 18 hoping to see absorption from cold gas in the largest H II region in the galaxy. However, we see no Na D absorption and our spectra show a relatively featureless continuum, with a prominent hydrogen Balmer series and weak emission from [O III] ($\lambda\lambda 4363, 4959, 5007$), and only the stronger line from the [S II] doublet at $\lambda 6716$. We can place an upper limit on the column density of Na D of $\sim 10^{12} \text{ cm}^{-2}$, using a S/N ~ 4 from the continuum and an assumed line width of 30 km s^{-1} – on par with the line widths in other dwarfs. This translates to an upper limit of $2.1 \times 10^9 M_\odot (R/970 \text{ pc})^2$ on the mass of neutral gas in I Zw 18, if the cold, neutral gas is entrained in the 970 pc superbubble parameterized in Martin 1998. It would be somewhat surprising to find even this much neutral sodium in this bubble, considering the incredibly low metallicity of this galaxy. Using a metallicity of 2% solar, we find an upper limit on the H I column of $\lesssim 10^{22} \text{ cm}^{-2}$. This is calculated given an abundance $[Na/H] = -1.70$, which is consistent with the value of $[Fe/H] = -1.76$ derived from *FUSE* observations by Aloisi et al. (2003). This roughly result agrees with previous measurements of the H I column of a few $\times 10^{21} \text{ cm}^{-2}$ (Aloisi et al. 2003; Lecavelier des Etangs et al. 2004; van Zee et al. 1998), and is consistent with a $\sim 2\%$ solar abundance of sodium.

5. Conclusions

We have obtained high-resolution Echelle spectra of six dwarf starburst galaxies, NGC 1614, and M82 in order to study the cold interstellar gas in dwarf starbursts. Interstellar neutral sodium column densities were obtained by measuring the equivalent width of the Na D absorption doublet. We find that out of the eight galaxies, NGC 1569, NGC 1614, NGC 4214-2, NGC 4449, and M82 unambiguously show interstellar sodium absorption, while NGC 2363, NGC 4214-1, NGC 5253, and I Zw 18 do not. The dwarf galaxies NGC 1569, NGC 4214, and NGC 4449 exhibit single-component outflows of neutral gas. NGC 1614 and M82 have multiple interstellar components, some outflowing and some infalling, and both galaxies show more absorption from outflowing gas than any dwarf galaxy.

The dwarf galaxies show trends similar to brighter, larger galaxies, but on a smaller scale. While samples of LIRGs and ULIRGs are shown to have average outflow speeds of $\sim 100 \text{ km s}^{-1}$ (HLSA) and $\sim 700 \text{ km s}^{-1}$ (Rupke et al. 2002; Martin & Armus 2004), respectively, the

three dwarfs show an average outflow speed of only $\sim 30 \text{ km s}^{-1}$. Additionally, most ULIRGs (e.g. 73% in Rupke et al. 2002) show an outflow, whereas only half of the galaxies in our sample have an outflow region. Spectral lines in dwarf galaxies also have smaller velocity spreads.

It is particularly interesting to see how complex the absorption line spectra become at high resolution. M82 is an excellent example of an absorption line system previously believed to be a single pair of lines, but within each member of the doublet we find a wealth of structure. We resolve at least five line pairs, showing the incredibly complicated nature of the CNM in this galaxy. This is a very intriguing result and prompts us to wonder how many of the galaxies in previous samples could be resolved into complex systems of multiple components. NGC 1614 shows complex absorption as well, though it has a far smoother profile in Na D (and K I) than M82. The three dwarfs with outflows do not seem to exhibit this behavior, showing far simpler spectra.

For the first time we are able to combine measurements of the kinematics of the warm, ionized gas in emission with absorption spectra of the cold, neutral gas. For sightlines intersecting a single shell, we can determine whether the ionization front is trapped inside the shock front. This works extremely well for NGC 2363, which is a simple expanding bubble with an ionization front that has expanded beyond the shock front. NGC 4214-2 also presents a relatively simple shell, and this galaxy also shows Na D absorption. From the kinematics we postulate that the ionization front is expanding faster than the shock front, though it has clearly not “caught up” yet, as there is still a concentric, outer expanding bubble of cold, neutral gas. In other words, the ionization front is still trapped in the shell. The kinematics of Na D and $H\alpha$ are very different in other galaxies, and cannot be easily explained by this straightforward picture.

Combining our measurements of Na I column density with previous observations of superbubbles and supershells in the sample galaxies, we have parameterized the mass of neutral gas (or a limiting case thereof) flowing out of the starbursting region. Using a simple spherical shell model, we find the total neutral gas outflow masses to be roughly 10^6 to $10^{10} M_{\odot}$. NGC 4449 shows far more outflowing cold gas than any other dwarf galaxy. Compared to the measurements of outflowing warm and hot gas from these galaxies (Martin 1998), it is likely that the bulk of the energy in the outflow is carried by the warm and hot gas, rather than cold gas.

Financial support was provided by the David and Lucille Packard Foundation and the Alfred P. Sloan Foundation. This research has made use of the NASA/IPAC Extragalactic Database (NED) which is operated by the Jet Propulsion Laboratory, California Institute of

Technology, under contract with the National Aeronautics and Space Administration. This research has made use of the NASA Astrophysics Data System abstract service. The authors wish to recognize and acknowledge the very significant cultural role and reverence that the summit of Mauna Kea has always had within the indigenous Hawaiian community. We are most fortunate to have the opportunity to conduct observations from this mountain. We appreciate comments and clarifications from an anonymous referee.

REFERENCES

- Aloisi, A., Savaglio, S., Heckman, T. M., Hoopes, C. G., Leitherer, C., & Sembach, K.R. 2003, *ApJ*, in press
- Alonso-Herrero, A., Engelbracht, C. W., Rieke, M. J., Rieke, G. H., & Quillen, A. C. 2001, *ApJ*, 546, 952
- Bajaja, E., Huchtmeier, W. K., & Klein, U. 1994, *A&A*, 285, 385
- Barlow, T. A., & Sargent, W. L. W. 1997, *AJ*, 113, 136
- Becker, R., Henkel, C., Bomans, D. J., & Wilson, T. L. 1995, *A&A*, 295, 302
- Bica, E., Pastoriza, M., Da Silva, L., Dottori, H., & Maia, M. 1991, *AJ*, 102, 1702
- Bushouse, H. A. 1987, *ApJ*, 320, 49
- Calzetti, D., Meurer, G. R., Bohlin, R. C., Garnett, D. R., Kinney, A. L., Leitherer, C., & Storchi-Bergmann, T. 1997, *AJ*, 114, 1834
- Cameron, A. G. W. 1973, *SSRv*, 15, 121
- Casoli, F., Dupraz, C., Combes, F., & Kasez, I., 1991, *A&A*, 251, 1
- Cerviño, M., & Mas-Hesse, J. M. 1994, *A&A* 284, 789
- Dahlem, M., Weaver, K. A., & Heckman, T. M. 1998, *ApJS*, 118, 401
- Gonzalez-Delgado, R., Leitherer, C., Heckman, T., Lowenthal, J., Ferguson, H., & Robert, C. 1998, *ApJ*, 495, 698
- Hartmann, D. & Burton, W. B. 1997, *Atlas of Galactic Neutral Hydrogen* (New York: Cambridge University Press)
- Heckman, T., Lehnert, M., Strickland, D., & Armus, L. 2000, *ApJS*, 129, 493 (HLSA)
- Huchra, J.P., Geller, M.J., Gallagher, J., Hunter, D., Hartmann, L., Fabbiano, G., & Aaronson, M. 1983, *ApJ*, 274, 125
- Hunter, D. A., Wilcots, E. M., van Woerden, H., Gallagher, J. S., & Kohle, S. 1998, *ApJ*, 495, L47
- Jacoby, G., Hunter, D., & Christian, C. 1984, *ApJS*, 56, 257

- Karachentsev, I. D., Makarov, D. I., & Huchtmeier, W. K. 1999, *A&AS*, 139,97
- Kobulnicky, H. A., & Skillman, E. D. 1995, *ApJ*, 454, L121
- . 1996, *ApJ*, 471, 211
- Kriss, G. 1994, ASP Conf. Ser. 61, in *Astronomical Data Analysis Software and Systems III*, ed. D. R. Crabtree, R. J. Hanisch, & J. Barnes (San Francisco: ASP), 437
- Kuntz, K. D. & Danly, L. 1996, *ApJ*, 457, 703
- Lecavelier des Etangs, A., et al. 2004, *A&A*, 413, 131
- Legrand, F., Tenorio-Tagle, G., Silich, S., Knuth, D., & Cerviño, M. 2001, *ApJ*, 560, 630
- Lehnert, M. D., & Heckman, T. M. 1996, *ApJ*, 472, 546
- Lehnert, M. D., Heckman, T. M., & Weaver, K. A. 1999, *ApJ*, 523, 575
- Leitherer, C., Vacca, W. D., Conti, P. S., Filippenko, A. V., Carmelle, R., & Sargent, W. L. W. 1996, *ApJ*, 465, 717
- Leitherer, C. et al. 1999, *ApJS*, 123, 3
- Lequeux, J., Peimbert, M., Rayo, J. F., Serrano, A., & Torres-Peimbert, S. 1979, *A&A*, 80, 155
- Lequeux, J., Knuth, D., Mas-Hesse, J., & Sargent, W. 1995, *A&A*, 301, 18
- Lo, K.-Y., Cheung, K., Masson, C., Phillips, T., Scott, S., & Woody, D. 1987, *ApJ*, 312, 574
- Luridiana, V., Peimbert, M., & Leitherer, C. 1999, *ApJ*, 527, 110
- MacKenty, J. W., Maíz-Apellániz, J., Pickens, C. E., Norman, C. A., & Walborn, N. R. 2000, *AJ*, 120, 3007
- Marlowe, A. T., Heckman, T. M., Wyse, R. F. G., & Schommer, R. 1995, *ApJ*, 438, 563
- Martin, C. L. 1996, *ApJ*, 465, 680
- . 1998, *ApJ*, 506, 222
- . 1999, *ApJ*, 513, 156
- Martin, C. L. & Armus, L. 2004, in preparation

- Martin, W. C. & Zalubas, R. 1981, *J. Phys. Chem. Ref. Data*, 10, 153
- Martin, C. L., Kobulnicky, H. A., & Heckman, T. M. 2002, *ApJ*, 574, 663
- McIntyre, V. J. 1998, *Publications of the Astronomical Society of Australia*, 15, 157
- Meier, D. S., Turner, J. L., Crosthwaite, L. P., & Beck, S. C. 2001, *AJ*, 121, 740
- Morton, D. C. 1991, *ApJS*, 77, 119
- Mühle, S., Hüttemeister, S., Klein, U., & Wilcots, E. M. 2001, *Astronomische Gesellschaft Meeting Abstracts*, 18, 546
- Neff, S. G., Hutchins, J. B., Standord, S. A., & Unger, S. W. 1990, *AJ*, 99, 1088
- Ohyama, Y., et al. 2002, in *ASP Conf. Ser. 289, The Proceedings of the IAU 8th Asian-Pacific Regional Meeting*, ed. S. Ikeuchi, J. Hearnshaw, & T. Hanawa (San Francisco: ASP), 285
- Papaderos, P., Loose, H.-H. Thuan, T. X., & Fricke, K. J., 1996, *A&AS*, 120, 207
- Phillips, A. 1993, *AJ*, 105, 486
- Roy, J.-R., Boulesteix, J., Joncas, G., & Grundseth, B. 1991, *ApJ*, 367, 141
- Rupke, D. S., Veilleux, S., & Sanders, D. B. 2002, *ApJ*, 570, 588
- Sargent, W. L. W., & Fillipenko, A. V. 1991, *AJ*, 102, 107
- Savage, B. D., & Sembach, K. R. 1991, *ApJ*, 379, 245
- . 1996, *ARA&A*, 34, 279
- Silich, S. A., & Tenorio-Tagle, G. 1998, *MNRAS*, 299, 249
- Skillman, E. D., Kennicutt, R. C., & Hodge, P. W. 1989, *ApJ*, 347, 875
- Sofue, Y. 1997, *PASJ*, 49, 17
- Spitzer, L. 1968, *Diffuse Matter in Space* (New York: Interscience Publication)
- . 1978, *Physical Processes in the Interstellar Medium* (New York: Wiley-Interscience)
- Spitzer, L. & Fitzpatrick, E. L. 1995, *ApJ*, 445, 196
- Stil, J. M., & Israel, F. P. 2002, *A&A*, 392, 473

- Storchi-Bergmann, T., Calzetti, D., Kinney, A. L. 1994, ApJ, 429, 572
- Summers, L. K., Stevens, I. R., Strickland, D. K., & Heckman, T. M. 2003, MNRAS, 342, 690
- Umeda, H., Nomoto, K., Tsuru, T. G., & Matsumoto, H. 2002, ApJ, 578, 855
- van Zee, L., Westpfahl, D., Haynes, M. P., & Salzer, J. J. 1998, AJ, 115, 1000
- Vogt, S. S., et al. 1994, Proc. SPIE, 2198, 362
- Wakker, B. P. & Mathis, J. S. 2000, ApJ, 544, L107
- Wei, A., Walter, F., Neininger, N., & Klein, U. 1999, A&A, 345, L23
- Wills, K. A., Pedlar, A., & Muxlow, T. W. B. 2002, MNRAS, 331, 313

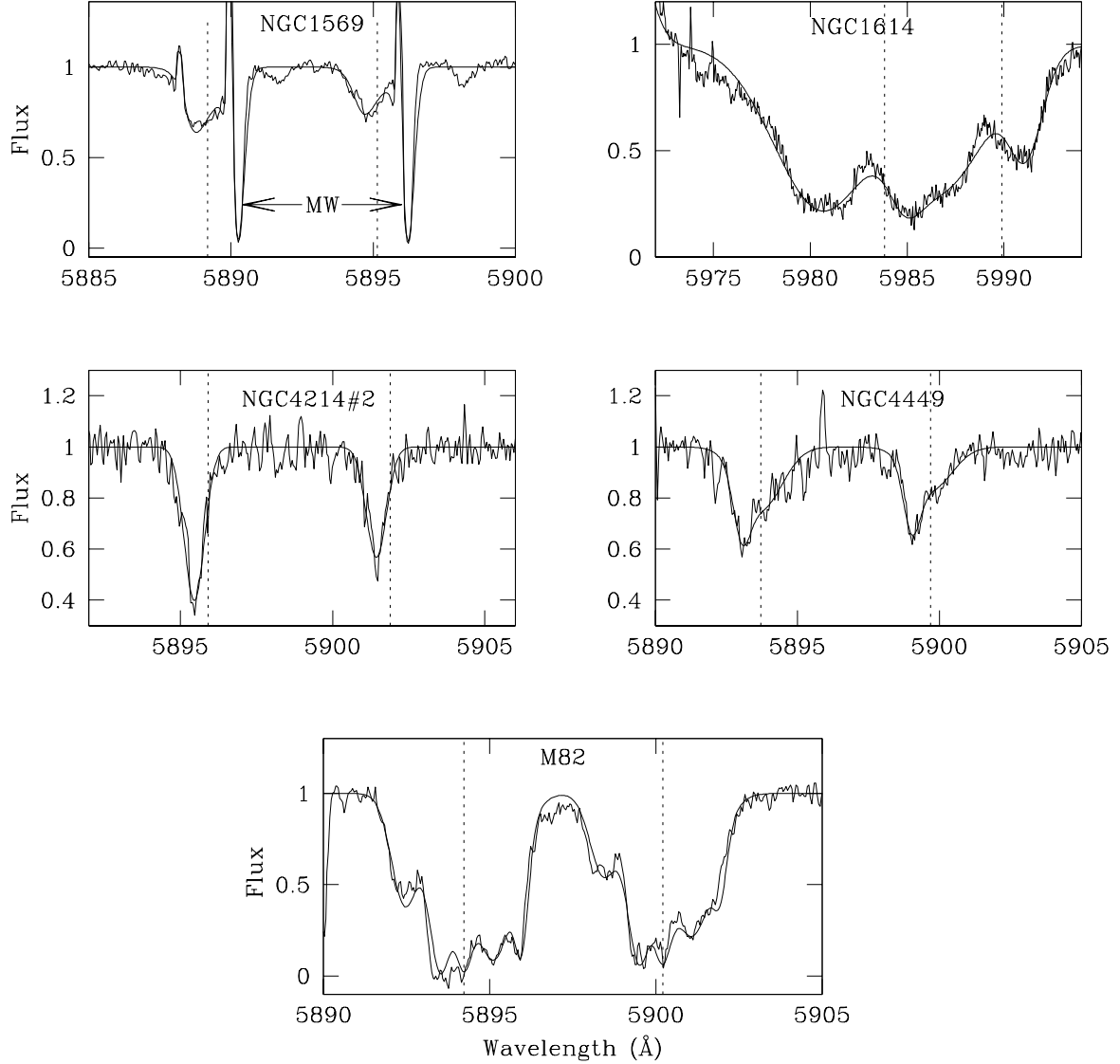


Fig. 1.— Normalized spectra of the Na D absorption line profile in the five galaxies in our sample where sodium was detected. The solid line plotted over the data is the fit from the SPECFIT program. The dotted lines represent the wavelengths corresponding to the systemic velocity for each of the Na D lines, which is the velocity given by the stellar Mg I absorption, H I rotation curves, or CO emission. The narrow emission and absorption in NGC 1569 are due to the atmosphere and the Galaxy, respectively, and are shown in detail in Figure 5.

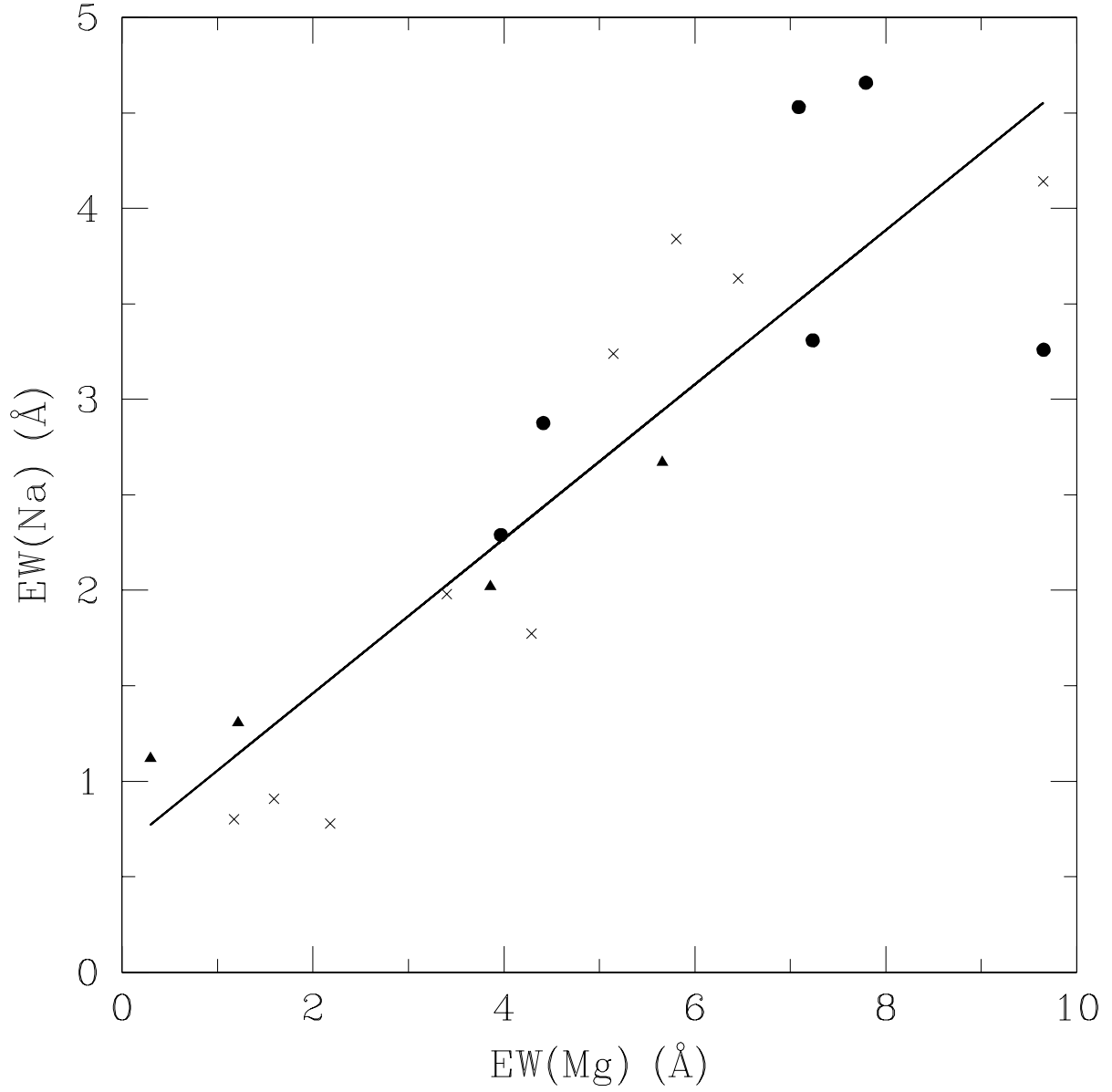


Fig. 2.— Total equivalent width of the Mg I absorption triplet versus that of the Na I doublet using data from Jacoby, Hunter, & Christian (1984). The relevant stars for this application are cooler ones in luminosity classes III (crosses), II (filled triangles), and I (filled circles). The solid line is a linear least-squares fit to the data. This gives us a slope of 0.40 and a y-intercept of 0.65.

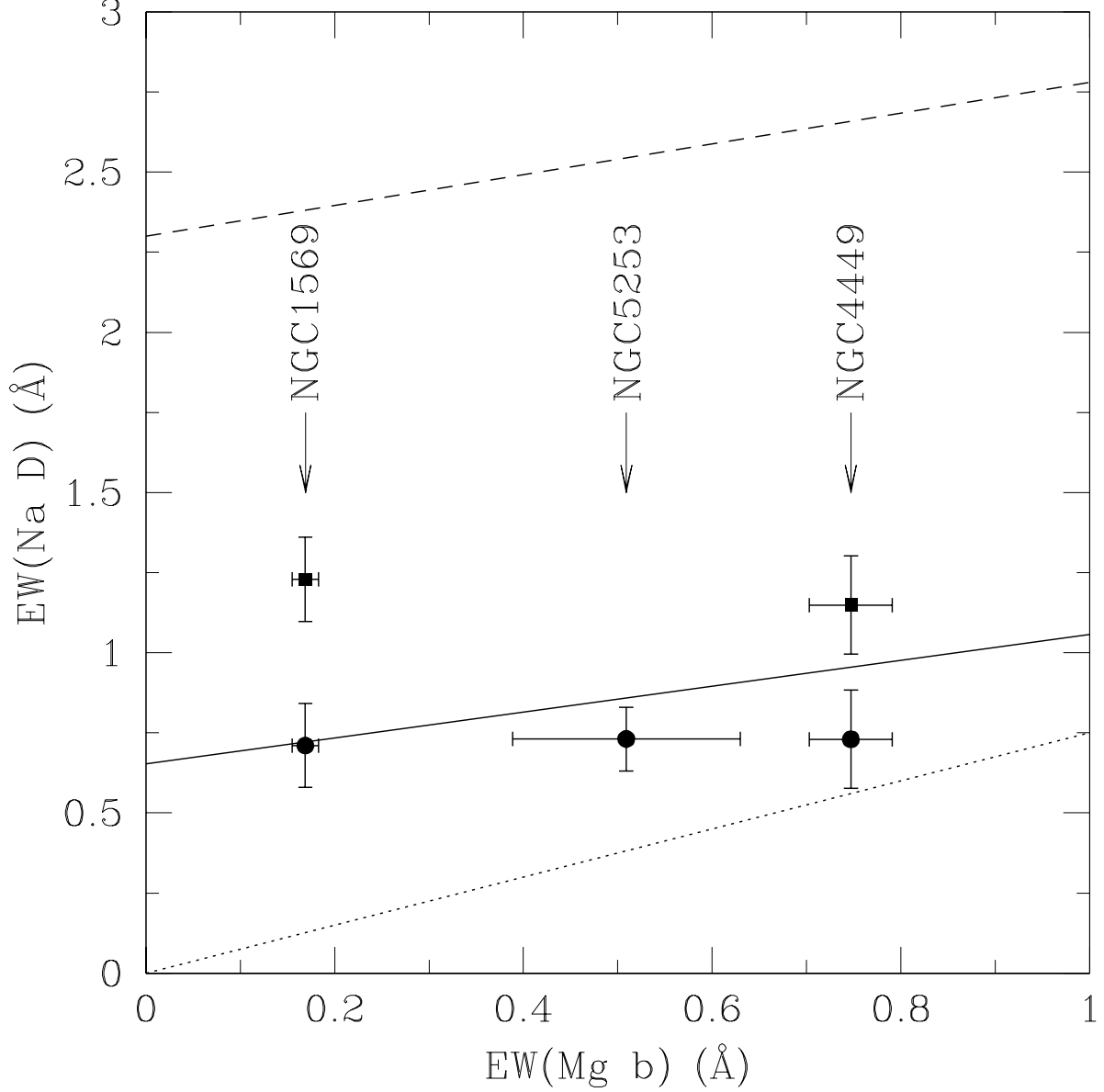


Fig. 3.— Total equivalent width of the Mg I absorption triplet versus stellar Na I (filled circles), and total (stellar + interstellar) Na I (filled squares), for the three galaxies showing Mg I absorption. Only one point is shown for NGC 5253 because it has a single stellar component. The dotted line is the model used by HLSA, the dashed line is the fit given for elliptical galaxies by Bica et al. (1991), and the solid line is our fit to the stellar spectra of Jacoby et al. (1984).

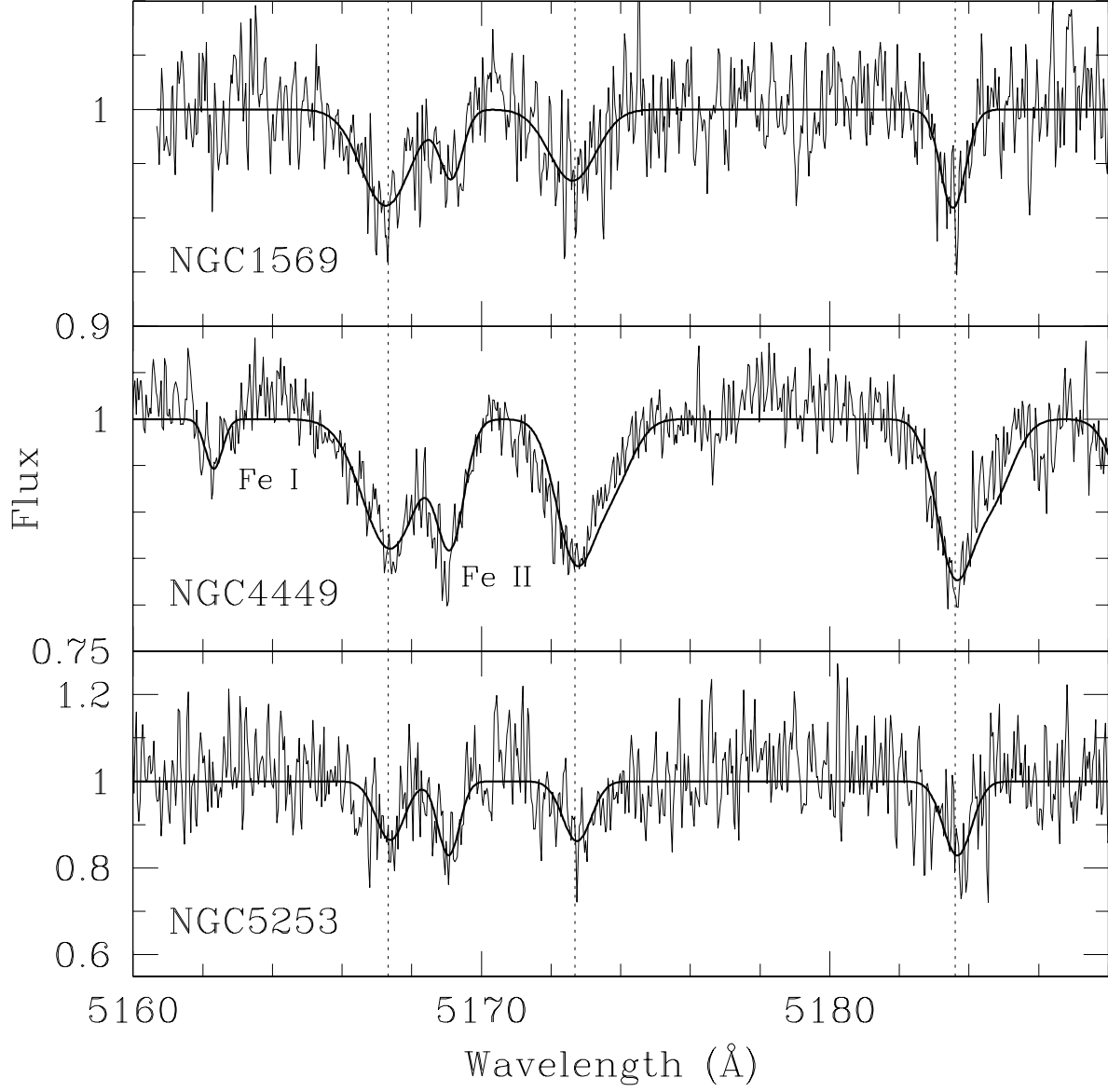


Fig. 4.— Mg I spectra for NGC 1569, NGC 4449, and NGC 5253, corrected for the systemic velocity by dividing by $(1+v_{sys}/c)$. The vertical lines indicate the rest wavelengths of the Mg b band triplet lines. The other stellar absorption lines present are Fe I (5162.3 Å) and Fe II (5169.0 Å).

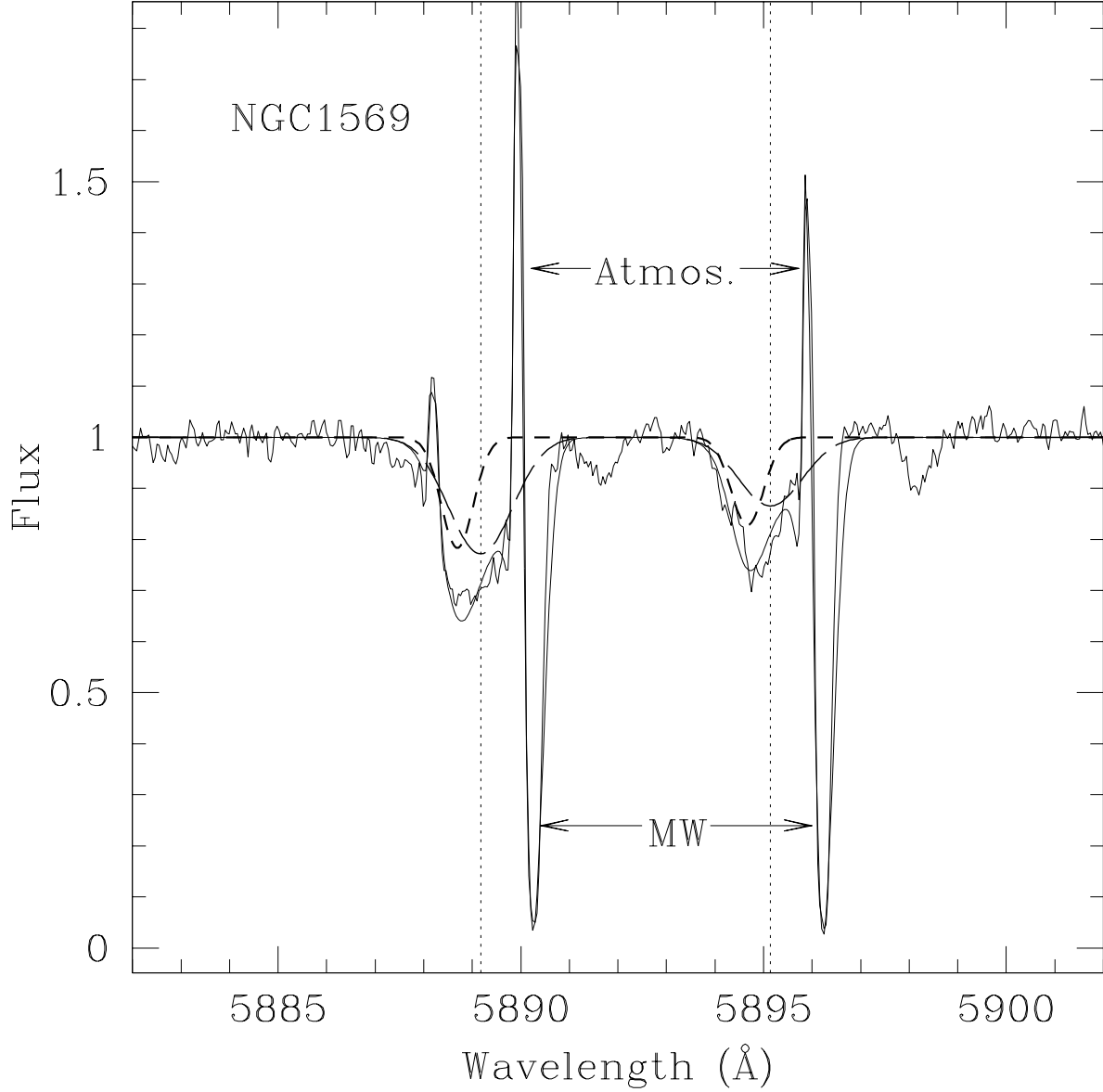


Fig. 5.— Na D spectrum in NGC 1569, with no background subtraction. Vertical dotted lines are at the systemic velocity given by Mg I absorption (-39.7 km s^{-1}). Overplotted are the model obtained using SPECFIT (solid line), the components of interstellar sodium corresponding to the K I absorption (short-dashed line), and the components of stellar sodium corresponding to the Mg I absorption (long-dashed line). The emission is at 0 km s^{-1} , due to sodium in the atmosphere, and is labelled “Atmos.” The deep, narrow absorption is due to sodium in the galactic plane and is labelled “MW.”

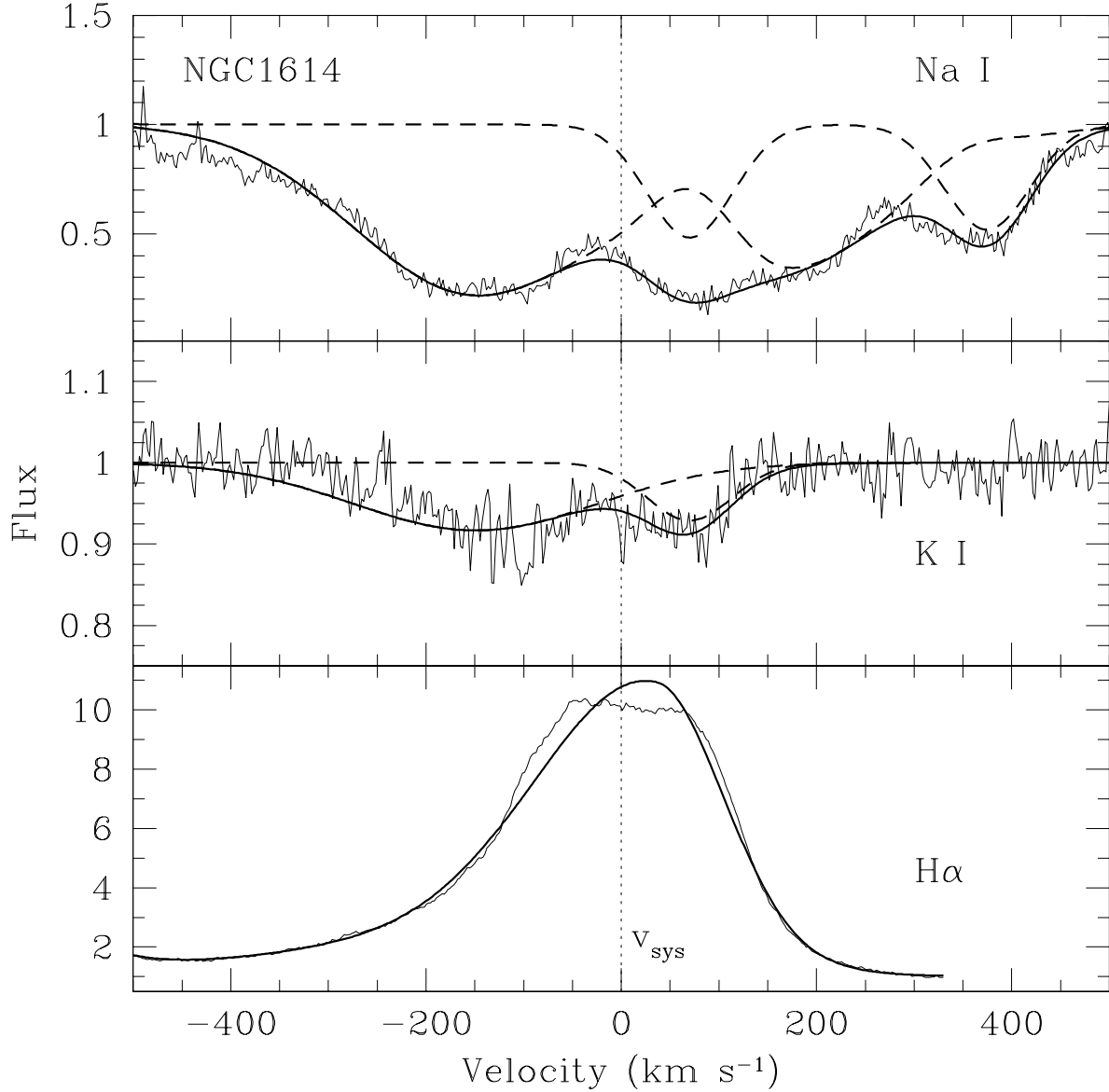


Fig. 6.— Na I, K I, and H α spectra for NGC 1614. The solid lines are the Gaussian models provided by SPECFIT, the dashed lines in Na I and K I show the components. In sodium, all the Na D components overlap each other, whereas K I shows only the 7665 \AA line. Note the prominently blueshifted and redshifted components of the absorption features (at -149 km s^{-1} and $+70$ km s^{-1} , respectively), as well as the complete lack of correlation with the H α emission. The dotted line shows the systemic velocity, as determined from CO observations by Casoli et al. (1991). The Na I was converted to a velocity scale using the wavelength of the blue member of the Na D doublet.

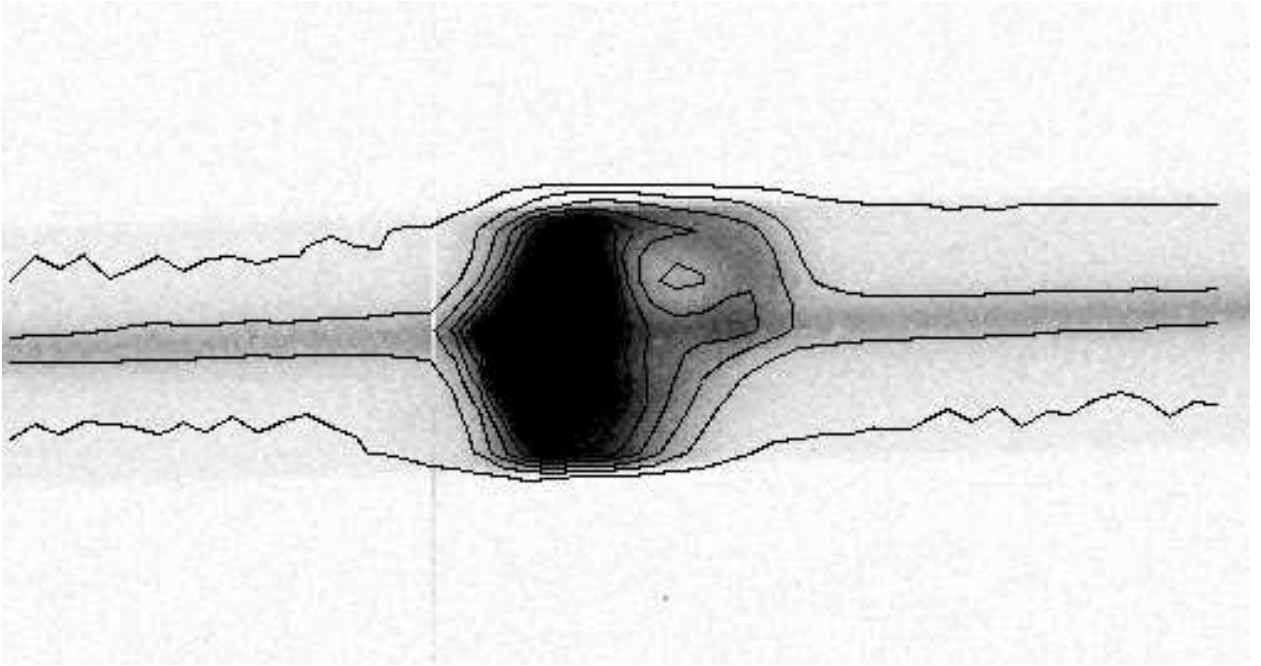


Fig. 7.— $H\alpha$ echellegram for NGC 4214-2. Wavelength increases to the right. The vertical axis is spatially along the slit; the aperture is $10''$ long (175 pc at a distance of 3.6 Mpc). The total width of the $H\alpha$ feature is 5.7 \AA , or 260 km s^{-1} . The “hole” seen on the red side of the spectral feature measures approximately $2''$ (35 pc) by 28 km s^{-1} . The contour spacing is linear.

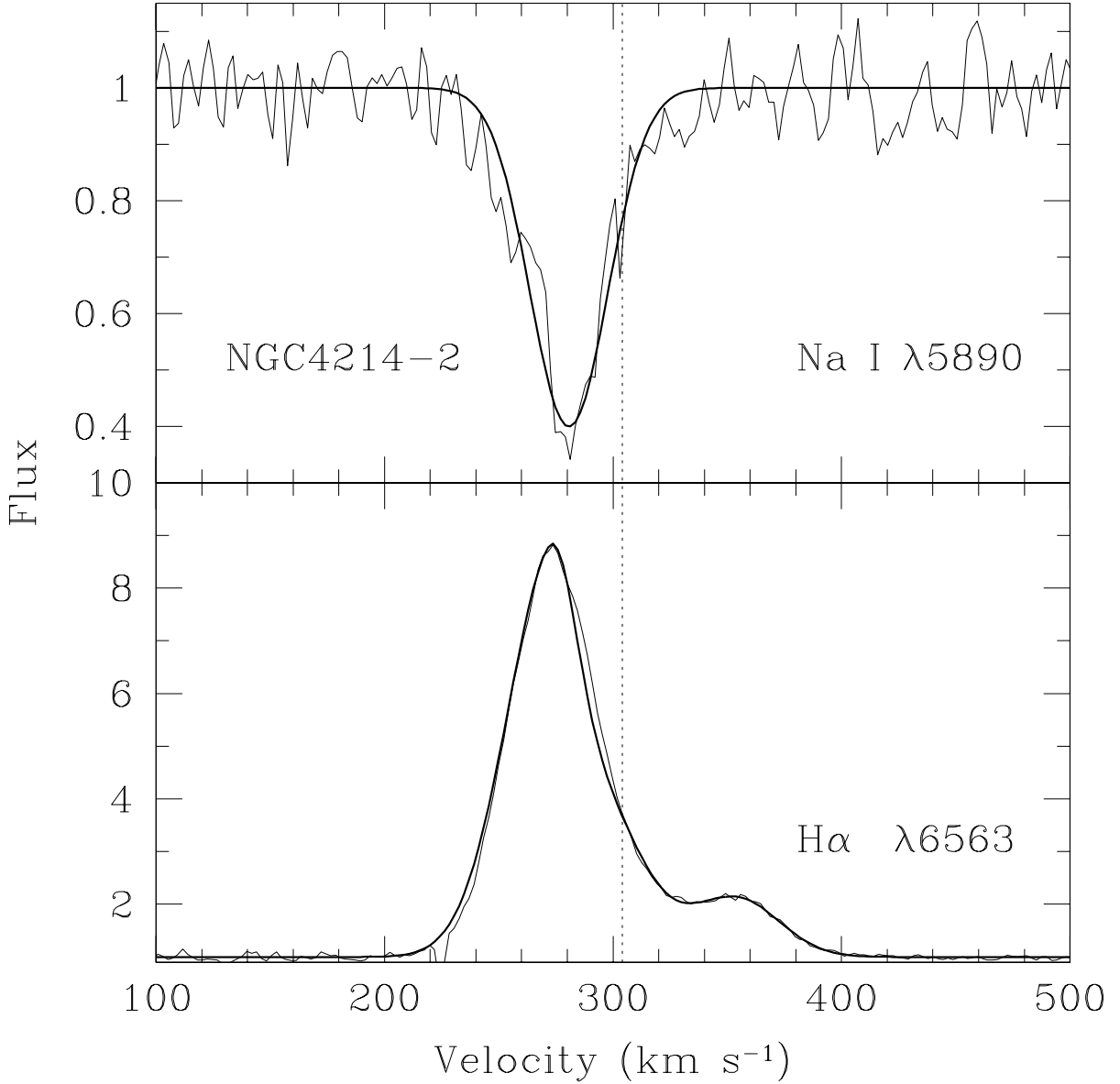


Fig. 8.— Normalized Na D and H α spectra in velocity space for NGC 4214-2. The spectral fit plotted over the data with a solid line. The dotted line is the systemic velocity (304 km s⁻¹) as given by ¹²CO (Becker et al. 1995). The top panel shows the blue (stronger) line of the Na D absorption doublet ($\lambda 5890$), which is blueshifted by ~ 24 km s⁻¹. The bottom panel shows the H α emission line, which is bimodal with one redshifted component and a brighter component blueshifted by ~ 30 km s⁻¹. The difference in velocity suggests that the ionization front is expanding faster than the shock front, although there is still a region of cold, neutral gas between the two fronts.

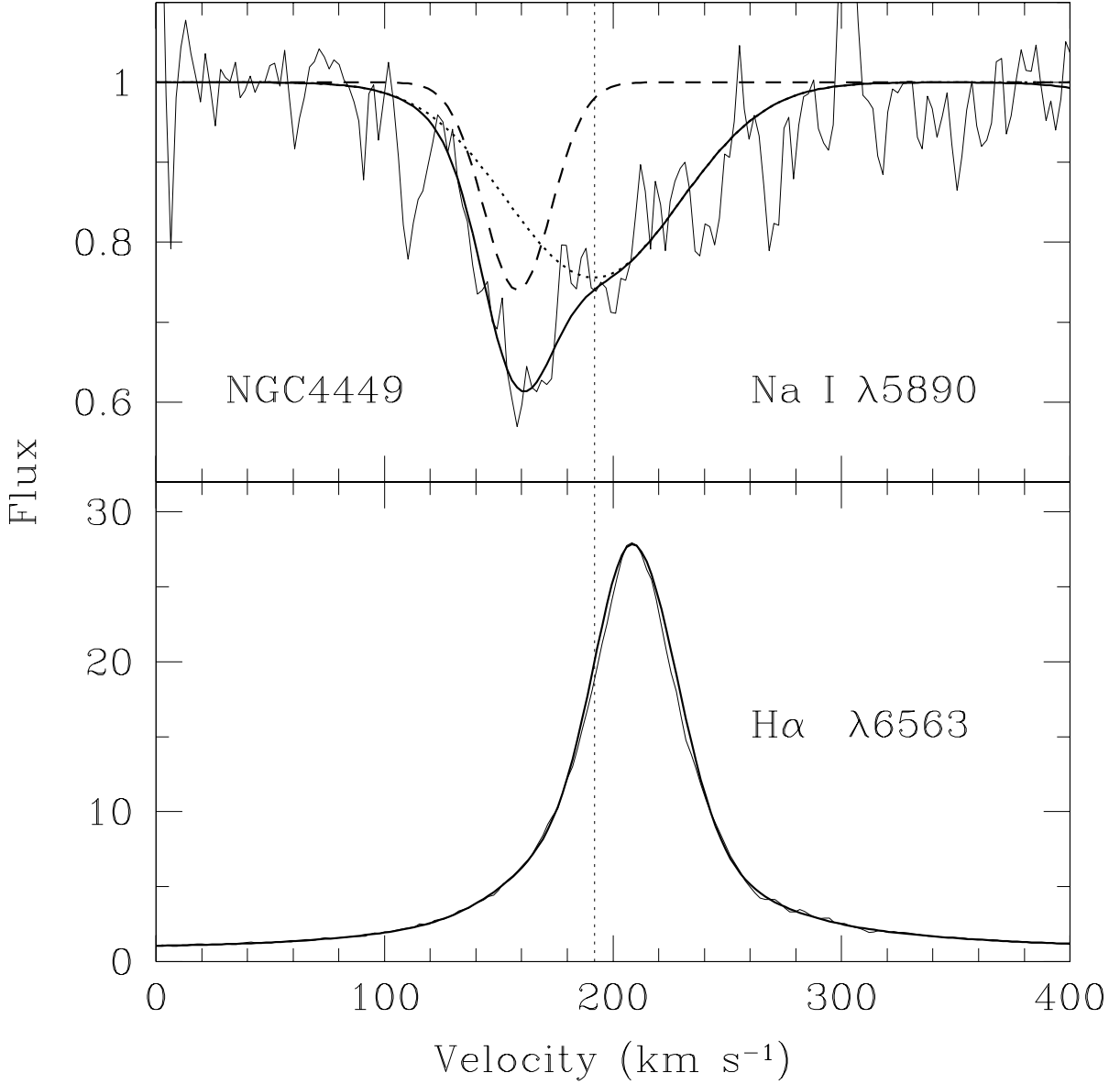


Fig. 9.— The normalized spectra in velocity space for NGC 4449 with spectral fit plotted over with a solid line. The dotted line is the systemic velocity as given by Mg b band absorption in this paper (192 km s^{-1}). The top panel shows the blue (stronger) line of the Na D absorption doublet ($\lambda 5890$), which is blueshifted by $\sim 34 \text{ km s}^{-1}$ and fit with a stellar component at the systemic velocity. The bottom panel shows the H α emission line, which is fit with one component at the systemic velocity and a brighter component redshifted by $\sim 17 \text{ km s}^{-1}$.

Table 1. THE SAMPLE OF GALAXIES

Galaxy	Type	v_{sys} (km s ⁻¹)	v_{rot}^a (km s ⁻¹)	d (Mpc)	M_B	M(H I) (10 ⁷ M _⊙)	W_{NaD}^b (Å)	References
NGC 1569	IBm	-40	28	2.2	-17.26	5.9	0.92	1, 2
NGC 1614	SB(s)c pec	4730	210	64.0	-20.84	170	11.25	3, 4
NGC 2363	IB(s)m	70	53	3.6	-16.75	79	...	5, 2
NGC 4214	IAB(s)m	304	35	3.6	-17.65	110	1.05 ^c	6, 2
NGC 4449	IBm	192	65	3.6	-17.86	135	0.34	1, 2
NGC 5253	Im(pec?)	389	<15	4.1	-17.62	20	0.73	1, 2
M82	I0	214	135	3.6	-18.95	88	7.98	7, 8
I Zw 18	...	761	50	10.0	-13.84	2.6	...	9, 10

^aRotational velocity for NGC 1614 is from global CO 115 GHz emission-line profiles using the half-width at 20% of the peak intensity and then correcting for the inclination (HLSA). All others are from Martin (1998) and references therein.

^b W_{NaD} given is the total equivalent width of the entire Na D absorption feature, i.e. both doublet lines, regardless of the source; it is uncorrected for covering factor.

^c W_{NaD} given for NGC 4214 is total sodium equivalent width for both NGC 4214-1 and NGC 4214-2, which have values of 0.18 Å and 0.86 Å, respectively.

Note. — Systemic velocity value in the third column is from the first reference in the last column. Absolute blue magnitude M_B is calculated from the RC3 magnitude B_T^0 , except in the case of NGC 1614, which is calculated from the value given in the NASA Extragalactic Database (NED) and corrected for Galactic/foreground extinction. H I mass is from the second reference in the last column.

References. — (1) This paper. (2) Karachentsev, Makarov, & Huchtmeier 1999. (3) Casoli et al. 1991. (4) Bushouse 1987. (5) NED. (6) Becker et al. 1995. (7) Lo et al. 1987. (8) Sofue 1997. (9) Aloisi et al. 2003. (10) Papaderos et al. 1996.

Table 2. INTERSTELLAR NA I COLUMN DENSITIES

Galaxy	$v-v_{sys}$ (km s ⁻¹)	W_{5890} ^a (Å)	Doublet Ratio	FWHM (km s ⁻¹)	C_f	Z/Z_{\odot} ^b	$N(\text{Na I})$ (10 ¹² cm ⁻²)
NGC 1569	-24	0.20	1.38	39.7	0.23	0.25	0.62 ± 0.22
NGC 1614	-149	4.85	1.15	294.7	0.80	0.70	42.52 ± 0.20
	+70	1.13	1.08	102.7	0.52	...	58.93 ± 0.20
NGC 4214-2	-23	0.50	1.39	39.9	0.71	0.25	2.2 ± 0.28
NGC 4449	-34	0.17	1.07	30.9	0.27	0.25	50.9 ± 0.28
M82	-91	0.62	1.36	49.1	0.69	1.0	3.0 ± 0.17
	-35	1.03	1.11	47.2	1.00	...	1.7 ± 0.17
	+4	0.77	1.13	36.7	1.00	...	7.7 ± 0.17
	+45	1.52	1.19	78.5	1.00	...	9.4 ± 0.17
	+86	0.46	1.98	24.6	1.00	...	2.4 ± 0.17
NGC 2363	...	0.11	0.25	<0.57
NGC 4214-1	...	0.04	0.25	<0.37
NGC 5253	...	0.07	0.37	<0.20
I Zw 18	...	0.25	0.02	<1.27

Note. — Neutral sodium column density is contingent on ionization parameter and fractional depletion of sodium onto grains. These quantities are inversely proportional to the column density, and therefore the given values above are estimates in that respect. See section 3.3.

^a W_{5890} refers to the model fit of the blue line, in Angstroms, when interstellar in nature. When no interstellar Na D is seen, an upper limit is given. This measurement is uncorrected for covering factor, though a correction is included in the column density calculations.

^bMetallicity used is given in the following references: NGC 1569 – Martin et al. 2002; NGC 1614 – Storch-Bergmann, Calzetti, & Kinney 1994; NGC 2363 – Luridiana, Peimbert, & Leitherer 1999; NGC 4214 – Leitherer et al. 1996; NGC 4449 –

Skillman, Kennicutt, & Hodge 1989; NGC 5253 – Marlowe et al. 1995; M82 – Umeda et al. 2002, and references therein; I Zw 18 – Martin 1996. Solar abundances are defined in Cameron 1973.

Table 3. INTERSTELLAR K I COLUMN DENSITIES

Galaxy	$v-v_{sys}$ (km s ⁻¹)	W_{7665}^a (Å)	Doublet Ratio	FWHM (km s ⁻¹)	N(K I) (10 ¹² cm ⁻²)
NGC 1569	-24	0.38	1.38	39.7	1.9
NGC 1614	-149	0.68	1.15	294.7	6.0
	+70	0.20	1.08	102.7	8.2

Note. — Neutral potassium column density is contingent on ionization parameter and fractional depletion of potassium onto grains. These quantities are inversely proportional to the column density, and therefore the given values above are lower limits. See section 3.4.

^a W_{7665} refers to the model fit of the blue line, in Angstroms. This measurement is uncorrected for covering factor, though a correction is included in the column density calculations.

Table 4. OUTFLOW PROPERTIES

Galaxy	$v-v_{sys}$ (km s ⁻¹)	R_{shell}^a (pc)	M_{NaI} (M _⊙)	M_{HI}^b (M _⊙)
NGC 1569	-24	500	36±1	$4.3 \times 10^6 \pm 1.2 \times 10^5$
NGC 1614	-149	1000	10 ⁴ ±10	$4.2 \times 10^8 \pm 2 \times 10^5$
	+70	1000 ^c	$1.4 \times 10^4 \pm 10$	$5.8 \times 10^8 \pm 2 \times 10^5$
NGC 2363 ^d	...	122	<1.0	$< 2.4 \times 10^5$
NGC 4214-1 ^d	...	700	<42	$< 5 \times 10^6$
NGC 4214-2	-23	500	127±16	$1.5 \times 10^7 \pm 2 \times 10^6$
NGC 4449	-34	1000	$1.2 \times 10^4 \pm 65$	$1.4 \times 10^9 \pm 7.8 \times 10^6$
NGC 5253 ^d	...	870	<34	$< 2.8 \times 10^6$
M82	-91	743	381±21	$1.1 \times 10^7 \pm 6.5 \times 10^5$
	-35	286	32±3.2	$9.6 \times 10^5 \pm 9.6 \times 10^4$
	+4	500 ^c	450±10	$1.3 \times 10^7 \pm 3 \times 10^5$
	+45	500 ^c	540±10	$1.6 \times 10^7 \pm 3 \times 10^5$
	+86	500 ^c	140±10	$4.2 \times 10^6 \pm 3 \times 10^5$
I Zw 18 ^d	...	970	<275	$< 4.1 \times 10^8$

Note. — Masses and errors are computed assuming $f_D f_{ion} = 100$ and the radii given in the table. Metallicities used are given in Table 2. Errors resulting from deviations from the model itself (e.g. non-sphericity or other geometrical issues) are not included.

^aRadii used in superbubble mass calculations are referenced in text.

^bAtomic hydrogen mass. Calculated from M_{NaI} as discussed in §4.1.

^cRadii used for redshifted/infalling components in NGC 1614 and M82 are estimates based on the size of the expanding superbubbles.

^dMasses given for NGC 2363, NGC 4214-1, NGC 5253, and I Zw 18 are upper limits based on calculations detailed in the text and Table 2.